

# Analyst

Accepted Manuscript



This is an *Accepted Manuscript*, which has been through the Royal Society of Chemistry peer review process and has been accepted for publication.

*Accepted Manuscripts* are published online shortly after acceptance, before technical editing, formatting and proof reading. Using this free service, authors can make their results available to the community, in citable form, before we publish the edited article. We will replace this *Accepted Manuscript* with the edited and formatted *Advance Article* as soon as it is available.

You can find more information about *Accepted Manuscripts* in the [Information for Authors](#).

Please note that technical editing may introduce minor changes to the text and/or graphics, which may alter content. The journal's standard [Terms & Conditions](#) and the [Ethical guidelines](#) still apply. In no event shall the Royal Society of Chemistry be held responsible for any errors or omissions in this *Accepted Manuscript* or any consequences arising from the use of any information it contains.

## Applications of Two-Dimensional Infrared Spectroscopy

Amanda L. Le Sueur, Rachel E. Horness, Megan C. Thielges

### Motivation

The past decade has seen a surge in the development of multidimensional infrared (IR) spectroscopy. Because IR spectroscopy probes the structural degrees of freedom of a molecule, it directly characterizes the potential energy surface that describes a molecule's nuclear and electronic structure. Vibrational frequencies are also highly sensitive to molecular environments, and so IR spectroscopy is useful for characterization of local sites and their fluctuations within complex systems. Multidimensional methods provide richer information than is available from linear experiments. They are able, for example, to identify interactions between vibrational modes and to measure the temporal evolution of vibrational frequencies. The experiments of multidimensional IR spectroscopy are akin to those long-established in the field of NMR spectroscopy. Unlike NMR spectroscopy, which is typically limited to detection of species interconverting on millisecond and slower timescales, IR spectroscopy has the advantage of an inherently fast, sub-picosecond timescale that ensures detection of states that rapidly interconvert and enables direct measurement of fast structural and/or environmental fluctuations. IR spectroscopy is thus well suited for the study of condensed phase samples where structural and environmental fluctuations occur on very fast timescales. The combination of high temporal resolution and bond-specific structural detail distinctively provided by IR spectroscopy makes it a powerful experimental approach for the study of molecular structure and dynamics.

The recent development of multidimensional IR spectroscopy has positioned the methods for application in a wide variety of research areas in chemistry and biology. A number of recent reviews and texts offer excellent, comprehensive treatments of the theory and experimental aspects of the methods.<sup>1-8</sup> This minireview provides a brief outline of the general principles, experimental implementation, and information available from two-dimensional (2D) IR spectroscopy, one of the most prevalent multidimensional IR experiments. We first highlight recent representative studies of 2D IR spectroscopy applied to small molecule systems to illustrate the principal spectral features of 2D spectra and what they tell us about molecular structure and dynamics. We then present example applications of 2D IR spectroscopy toward characterization of more complex systems, such as of interest in biological and materials chemistry. Our intent is to present only a sample of the possible applications of 2D IR spectroscopy to communicate its advantages for addressing questions in chemistry and biology.

### Fundamentals of 2D IR spectroscopy

2D IR spectroscopy measures the correlation among the frequencies of the vibrations of a system and their time evolution. The experiment involves application of an IR pulse sequence that labels the system with its initial frequencies, allows the system to evolve, and then reads out the final frequencies. One axis of a 2D spectrum describes initial excited frequencies, while the orthogonal axis associates these frequencies with the final detected frequencies. The simplest case of a 2D spectrum of a single vibrational mode illustrates the additional information available from the second dimension. In the typical situation that the laser bandwidth encompasses both the 0-1 and 1-2 transition frequencies, a single vibrational mode leads to a pair of bands of opposite sign in a 2D spectrum (for example, see Fig. 1). Both of the bands appear along the initial excitation axis at the frequency of the 0-1 transition because they arise from the excitation of an initial ground state population. Along the detection axis, one band arises at the 0-1 frequency due to a combination of stimulated emission and ground state population reduction, while the other arises at the 1-2 frequency due to further excitation of the population in the first excited state. Thus a 2D IR spectrum of a single vibrational mode provides information about the correlation between its initial and final frequencies – in this specific example, between the initial 0-1 transition frequency and both the 0-1 and the 1-2 transition frequencies of the same mode.

1  
2  
3  
4  
5  
6  
7  
8  
9  
10  
11  
12  
13  
14  
15  
16  
17  
18  
19  
20  
21  
22  
23  
24  
25  
26  
27  
28  
29  
30  
31  
32  
33  
34  
35  
36  
37  
38  
39  
40  
41  
42  
43  
44  
45  
46  
47  
48  
49  
50  
51  
52  
53  
54  
55  
56  
57  
58  
59  
60

In a similar manner, the correlations between frequencies reported in 2D spectra elucidate the interaction between vibrational modes, interconversion between chemical species or environments, and intra- or intermolecular vibrational energy relaxation.<sup>5-7</sup> For example, cross-bands appear between the frequencies of two coupled modes, indicating that excitation at the frequency of one mode results in detection at the frequency of the other. The cross-band intensities reflect the strength of the coupling interaction, which in turn depends on the proximity and relative orientation of the coupled modes. The cross-bands are therefore highly sensitive to molecular structure and intermolecular interactions, and so are valuable for the assignment and interpretation of IR spectra, which can be very complex for even moderately sized molecules. Moreover, the high sensitivity of vibrational coupling to the distance and relative orientation of the modes enables generation of structural models of molecules.

Multiple bands can appear in a linear IR spectrum not only due to multiple vibrational modes, but also due to a single mode in distinct environments (*e.g.* resulting from conformational changes or chemical reactions). In these cases, cross-bands arise in a 2D spectrum at the frequencies associated with the different environments or chemical species if they interchange within the time of initial excitation and the time of detection in the acquisition of a 2D spectrum. The cross-bands due to such exchange processes grow in intensity over time on the timescale of the environmental fluctuation or chemical interconversion. In many situations, the different, interconverting species do not lead to distinct bands, but rather manifest as an inhomogeneously broadened band. 2D IR spectroscopy can be used to measure the evolution of these frequencies, referred to as spectral diffusion. Rather than distinct cross-bands, the interconversion of the associated states causes the 2D bands to become progressively less diagonally elongated with increasing time. As we discuss specific applications of 2D IR spectroscopy, we will point out how 2D spectra and their time evolution inform on these processes.

### Experimental implementation of 2D IR spectroscopy

The theory and experimental implementation of 2D IR spectroscopy, and multidimensional spectroscopy in general, have been comprehensively treated in recent reviews<sup>1-3</sup> and texts,<sup>4-7</sup> so a brief outline of a basic, conventional implementation of a 2D IR experiment is presented here. A 2D IR experiment involves temporally-controlled application of three ultrashort mid-IR pulses, which lead to a third-order polarization in the sample (Fig. 1). The times between the first and second excitation pulses, and between the second and third excitation pulses, are commonly referred to as the coherence time ( $\tau$ ) and the waiting time ( $T_w$ ), respectively. To acquire a single 2D IR spectrum,  $\tau$  is scanned for a fixed value of  $T_w$ . At a time  $\leq \tau$  after the third pulse, a third-order signal is generated by the sample in a unique (phase-matched) direction. This IR pulse is spatially filtered and heterodyne-detected by overlapping with another IR pulse, the local oscillator, which provides both signal amplification and phase information. Commonly, the combined pulses are frequency-dispersed onto an array detector, providing a direct measurement of the spectrum along the final detected frequency axis (alternately referred to as the  $\omega_m$ ,  $\omega_3$ , or probe axis). At each detected frequency, scanning  $\tau$  produces an interferogram. Numerical Fourier transformation of these interferograms generates the spectrum along the initial excitation frequency axis (alternately referred to as the  $\omega_\tau$ ,  $\omega_1$ , or pump axis). (Note that conventions for the placement of excitation and detection frequencies along the horizontal or vertical axes vary among research groups.) The evolution of the system during  $\tau$  labels the system with the initial frequencies. Detection of the heterodyned signal after the set waiting time  $T_w$  interrogates the final frequencies of the system. Thus, the resulting 2D IR spectrum reports on the correlation between the initial and final frequencies of the system after a time separation of  $T_w$ .

A number of variations of this conventional implementation of 2D IR spectroscopy have been developed.<sup>9-18</sup> For example, control of the polarization of the excitation pulses can provide orientational information about coupled modes or selectively highlight particular cross-bands.<sup>11, 12</sup> Upconversion of the mid-IR to visible frequencies enables the use of less expensive, more sensitive CCD array detectors available for visible frequencies.<sup>13, 14</sup> Frequency-domain versions of 2D IR spectroscopy are also well developed, including their application to a variety of systems.<sup>19-22</sup> An increasingly popular implementation of 2D IR spectroscopy uses pulse shaping

1  
2  
3 to generate and control the timing of the first two excitation pulses.<sup>9,23</sup> In fact, a 2D IR system  
4 that utilizes this design is now commercially available.<sup>24</sup> Pulse shaping methods enable  
5 significantly faster data acquisition, as well as phase-cycling procedures that can decrease data  
6 sampling demands or remove scattered light; however, these improvements come with the loss of  
7 the background-free signal generation in the conventional experiment. The advantages and  
8 disadvantages of different implementations of 2D IR spectroscopy have been discussed by several  
9 authors.<sup>9,25-27</sup> These and other advancements in the experimental methods of multidimensional IR  
10 spectroscopy over the past decade have established versatile tools for addressing a range of  
11 scientific questions.  
12

## 13 Applications of 2D IR spectroscopy

### 14 Applications to small molecule systems

15  
16 As the techniques of 2D IR spectroscopy have been established over the past decade, a variety of  
17 small molecule systems have been investigated, both due to inherent interest, as well as to develop  
18 small molecule probes to analyze more complex systems.<sup>28-33</sup> In the discussion that follows, we  
19 highlight a few examples in order to illustrate the information available from 2D IR spectroscopy.  
20  
21

### 22 Cross-band anisotropy of rapidly interconverting species

23 A central advantage of IR spectroscopy is the inherently fast, sub-picosecond timescale associated  
24 with the frequencies of IR transitions. 2D IR methods are thus complementary to the more  
25 established 2D NMR methods, which are typically limited to resolving structures that interconvert  
26 on millisecond or slower timescales. The high temporal resolution, combined with high structural  
27 sensitivity, make 2D IR spectroscopy suitable for the analysis of rapidly interconverting  
28 molecular structures. An interesting recent application is the structural analysis of molecular  
29 conformers in organic chemical reactions.<sup>34,35</sup> Knowledge of the structures adopted by small  
30 molecules is valuable for rationalizing and predicting chemical reactions, particularly those  
31 involving stereochemical control. For example, 2D IR spectroscopy has been applied to analyze  
32 the potential conformations adopted in the stereoselective Diels-Alder reaction of cyclopentadiene  
33 and *N*-crotonyloxazolidinone with Lewis acid catalyst SnCl<sub>4</sub>.<sup>35</sup> 2D spectra of equimolar solutions  
34 of the dieneophile substrate and SnCl<sub>4</sub> are shown in Fig. 2. As in a 2D NMR COSY spectrum,  
35 cross-bands indicate coupling interactions, and so identify bands due to a single conformer. The  
36 red and green grid lines in the spectra shown in Fig. 2 indicate bands due to the same species.  
37 The measurement of the cross-band anisotropy, the difference in the cross-band intensities for  
38 spectra obtained with parallel or perpendicularly polarized excitation beams, provides angular  
39 information about the transition dipoles of coupled vibrational modes that can be used to assign  
40 the structures of the populated conformers. The left panel of Fig. 2 shows the 2D IR spectrum  
41 obtained with parallel-polarized excitation bands. The right panel illustrates how select cross-  
42 bands can be annihilated by weighted subtraction of parallel- and perpendicular-polarized 2D  
43 spectra. In this example, 2D IR spectroscopy yields evidence that the dienophile substrate adopts  
44 the *anti* and *syn* conformers when free and bound to the SnCl<sub>4</sub> catalyst, respectively. The  
45 appearance of distinct bands for the two species illustrates the advantage of the fast inherent  
46 timescale of IR spectroscopy. In contrast, these conformers are in rapid exchange on the NMR  
47 timescale.  
48

### 49 Chemical exchange of ion complexes

50 The importance of ions in biology and a wide variety of other systems has prompted extensive  
51 investigation into ion pairing and the accompanying changes in solvent coordination.<sup>28,36-40</sup> The  
52 fast timescale of 2D IR spectroscopy enables direct, real-time monitoring of chemical exchange  
53 reactions when the exchange time is longer than or comparable to the vibrational lifetime of the  
54 monitored mode. As an illustration, 2D IR spectroscopy was used to study ion pair formation  
55 between magnesium (Mg<sup>2+</sup>) and calcium (Ca<sup>2+</sup>) cations with the thiocyanate anion (NCS<sup>-</sup>) and the  
56 anion exchange in the solvation shell.<sup>36</sup> The example spectra in Fig. 3 focus on the 2D band for  
57 the CN stretching vibration and illustrate the *T<sub>w</sub>*-dependent changes in its shape due to chemical  
58  
59  
60

1  
2  
3 exchange for aqueous solutions of NaNCS and  $\text{MgI}_2$ . At early  $T_w$ , two pairs of bands appear at  
4 distinct frequencies along the diagonal that reflect the free  $\text{NCS}^-$  and the contact ion pair with  
5  $\text{Mg}^{2+}$  (left panel, Fig. 3). As the  $\text{NCS}^-$  exchanges between the two states with increasing  $T_w$ ,  
6 cross-band intensity grows between the diagonal bands because the anion is excited at the  
7 frequency of one state but detected at the frequency of the other state (right panels, Fig. 3).  
8 Analysis of the time-dependent intensities of the cross-bands gives the timescales of the chemical  
9 exchange reaction. In this particular study, measurement of the exchange dynamics revealed  
10 different mechanisms for ion complex formation that depend on the identity of the cation,  
11 suggesting a dissociative mechanism for  $\text{Mg}^{2+}$  but an associative mechanism for  $\text{Ca}^{2+}$ . 2D IR  
12 spectroscopy has been similarly applied to characterize the ligand exchange and solvation  
13 dynamics of a wide variety of ion pairs.<sup>28, 39, 40</sup>  
14

### 15 Spectral diffusion due to solvent fluctuations

16 Multidimensional IR spectroscopy is particularly useful for the analysis of condensed phase  
17 samples, where the large heterogeneity in the local environments experienced by vibrational  
18 modes often leads to a continuous distribution in IR frequencies that result in broad, featureless  
19 linear absorption bands. 2D IR spectroscopy facilitates interpretation of such spectra by its ability  
20 to extract the underlying inhomogeneous distribution of frequencies that arise from environmental  
21 or structural heterogeneity. Furthermore, analysis of the time-dependent changes in the shape of  
22 the 2D bands reveals the dynamics of the interconversion within the inhomogeneous distribution  
23 of frequencies (spectral diffusion), providing information on the environmental fluctuations or  
24 structural dynamics of the molecule. As an example, Fig. 4 shows time-dependent 2D spectra of  
25 the NO stretching mode of sodium nitroprusside in ethylene glycol and water solvents.<sup>29</sup> At short  
26  $T_w$ , the 2D bands appear elongated along the diagonal (left panels, Fig. 4). This occurs because  
27 the states associated with the distribution of frequencies are not given sufficient time to  
28 interconvert. The frequencies initially excited are the same frequencies detected, and the  
29 diagonally elongated 2D bands reflect high correlation between the two frequency axes. As the  
30 time ( $T_w$ ) between labeling and detection of the frequencies is increased, the states have an  
31 increasingly longer time to interconvert. When this occurs, the initial and final frequencies of the  
32 species are no longer the same, and the loss of their frequency correlation causes the 2D band  
33 shape to become less elongated (right panels, Fig. 4). In comparison to the aqueous solution, the  
34 2D bands for the ethylene glycol solution show greater elongation at early  $T_w$  times and more  
35 slowly changing line shapes, indicating greater heterogeneity and slower dynamics of the NO  
36 environment in ethylene glycol. Procedures for quantifying the dynamics of the system by  
37 analysis of the 2D band shapes have been described.<sup>41</sup> As in this particular example, the  
38 measurement of spectral diffusion has been applied to study the dynamics of a variety of systems,  
39 including solvent, protein, and membrane environments.<sup>42-52</sup>  
40  
41

### 42 Vibrational energy transfer

43 2D IR spectroscopy can be used to analyze molecular structure via measurement of energy  
44 transport throughout a molecule.<sup>53-56</sup> For example, relaxation-assisted 2D IR spectroscopy, a dual-  
45 frequency variation of 2D IR spectroscopy, uses a laser pulse to deposit energy into a vibrational  
46 mode at one frequency, then monitors the dissipation of the excess energy through the molecule  
47 by detection of its influence on another vibrational mode at a different frequency.<sup>54</sup> Unlike cross-  
48 bands due to direct, strong coupling between spatially proximal or mechanically connected modes  
49 that appear with no waiting time, cross-bands due to relaxation-assisted processes grow in  
50 intensity with increasing waiting time as the excess energy deposited at one mode propagates  
51 throughout the molecule, typically via anharmonic coupling through the connecting bonds.  
52 Arrival of the energy at another mode shifts its frequency or absorption probability and results in  
53 cross-band amplitude. The time delay between energy deposition at the first mode and the  
54 maximum enhancement of its cross-band with a second mode depends on the bond connectivity  
55 between them. Correlation of bond distance and energy transport times can provide a molecular  
56 ruler of bond distances in a molecule. As an example, this method was applied to polyethylene  
57 glycol (PEG) oligomers of various length bearing azido and succinimide ester moieties as  
58  
59  
60

1  
2  
3 vibrational reporter tags.<sup>55</sup> The 2D IR spectrum in Fig. 5 shows a cross-band that arises from  
4 pumping at the azido frequency ( $2107\text{ cm}^{-1}$ ) and probing at the frequencies of the three carbonyl  
5 modes of the succinimide tag ( $1724, 1778, 1819\text{ cm}^{-1}$ ) 60 ps later. The energy deposited in the  
6 azido group dissipates throughout the PEG molecule via anharmonic through-bond coupling to  
7 lower frequency modes, which in turn couple to the carbonyl modes of the succinimide group, and  
8 contribute to a cross-band. In addition to advancing our fundamental understanding of vibrational  
9 energy relaxation mechanisms, relaxation-assisted 2D IR spectroscopy can correlate vibrational  
10 frequencies in molecules to assist in spectral assignment and provide bond connectivity and  
11 distance information for characterizing molecular structure. Recently, a related experiment has  
12 been demonstrated based on through-space resonance energy transfer between vibrational  
13 modes.<sup>56</sup> Analysis of the appearance of cross-bands due to energy transfer and their polarization  
14 dependence can provide angstrom-scale structural models of molecules.  
15

## 16 Applications to complex systems

### 17 Nucleic acids

18 DNA and RNA adopt secondary and tertiary structures that are essential to their function and the  
19 regulation of many biological processes. The high sensitivity of IR spectroscopy to structure and  
20 interactions, such as hydrogen bonding, and its ability to resolve highly dynamic, flexible  
21 structures afford great potential for the characterization of nucleic acids. Unfortunately, like other  
22 biomolecules, IR spectra of nucleic acids are highly congested. The spectral complexity hinders  
23 interpretation and limits the information attainable from IR spectra. Cross-bands in 2D spectra  
24 help alleviate this issue by providing additional information about the coupling between modes to  
25 assist spectral assignment. Indeed, 2D IR studies indicate that the vibrational modes of nucleic  
26 acids are more highly coupled than previously recognized.<sup>57-59</sup> For example, cross-bands in the  
27 2D spectra of the nucleotide monophosphates provide evidence that the commonly analyzed in-  
28 plane stretches are highly delocalized over the aromatic rings.<sup>57</sup> A better understanding of  
29 nucleotide vibrational bands and the factors that contribute to their changes will advance our  
30 ability to characterize more complex structures with linear or 2D IR spectroscopy.  
31

32 Although 2D IR spectroscopy of nucleic acids is less well developed than its application to  
33 peptide systems, it has been extended to chemically modified nucleic acid monomers and base  
34 pairs, as well as oligomers of poly-adenosine-thymidine (A-T) or guanosine-cytidine (G-C)  
35 sequences.<sup>57-65</sup> The capability of 2D IR spectroscopy to distinguish and identify vibrational  
36 modes, particularly the N-H modes, is critical in these studies. The first study of G-C base pairing  
37 found that a variety of factors, including both electrostatics and base stacking, contribute to the  
38 observed spectral changes.<sup>57, 66, 67</sup> Studies of A-T pairs with 2D IR spectroscopy reveal the  
39 presence of not only conventional Watson-Crick base pairing but also reverse and Hoogsteen base  
40 pairing interactions, further revealing nucleic acid complexity.<sup>58</sup> More complex samples of  
41 synthetic oligomers of repeating A-T or G-C at various levels of hydration have been investigated  
42 with 2D IR spectroscopy, making possible a more complete understanding of the vibrational  
43 modes and couplings.<sup>60, 61, 68</sup> These studies also find that water dynamics are influenced by the  
44 presence of nucleic acids, showing slower spectral diffusion compared to bulk water.  
45

46 One interesting application of 2D IR spectroscopy is the characterization of different tautomer  
47 populations of the nucleic acid bases.<sup>69-71</sup> Tautomerization of nucleic acids could be important in  
48 mechanisms of mutagenesis and generally in nucleic acid recognition, but its fast timescale has  
49 hindered its characterization under physiological conditions. Multiple tautomers have been  
50 detected in 2D IR studies of nucleic acid analogues, such as in a recent study of the modified  
51 nucleobase oxythiamine.<sup>69</sup> Cross-band patterns in 2D spectra due to coupling between vibrational  
52 modes permit the discrimination of the three tautomeric states, which is not possible with linear  
53 spectroscopy due to spectral congestion, nor with NMR spectroscopy due to their rapid  
54 interconversion. To illustrate, the appearance of cross-bands between only one of the two  
55 carbonyl stretching modes and a mode associated with a methyl group vibration provides  
56 evidence for the presence of two distinct keto forms (Fig. 6). The ability of 2D IR spectroscopy  
57 to generate richer spectral data and discern rapidly interconverting states could be very powerful  
58  
59  
60

1  
2  
3 for analysis of nucleic acid biophysics and elucidation of the mechanisms underlying biological  
4 function.  
5

## 6 **Peptide and protein structure and dynamics**

### 7 **Backbone structure and dynamics**

8  
9 2D IR spectroscopy has been extensively applied to the characterization of peptide and protein  
10 structures via the analysis of backbone vibrations.<sup>10, 72-79</sup> Spectral analysis typically focuses on the  
11 amide I vibrational mode, which primarily consists of C=O and N-H vibrations, due to its  
12 sensitivity to secondary structure and decoupling from protein side chain vibrations. Because the  
13 IR spectra of even small peptides are highly complex, site-selective <sup>13</sup>C and/or <sup>18</sup>O labeling is  
14 typically required to spectrally isolate vibrations due to individual residues. Structural  
15 information is principally derived from the distance and orientation dependence of transition  
16 dipole coupling between the amide I modes. Cross-bands are direct evidence for coupling.  
17 Coupling also leads to shifts in the transition frequencies of the coupled modes, which can  
18 manifest as band broadening when the bands are unresolved. These spectral changes are  
19 frequently analyzed to determine the strength of coupling between particular amide I modes,  
20 which in turn reflects their proximity and relative orientation.  
21

22 An important advantage of 2D IR spectroscopy is the fourth power dependence of the signal  
23 intensity on the transition dipole strength, compared to quadratic dependence for linear  
24 spectroscopy.<sup>80</sup> Because of this, the 2D spectral features of the amide I modes are more intense  
25 with respect to the background absorption in comparison with the linear spectrum. 2D IR  
26 spectroscopy also enables measurement of the inhomogeneous linewidths, as well as  
27 characterization of spectral diffusion, and so provides richer, more rigorous information than is  
28 available from linear spectroscopy. For instance, when all the spectral information obtained by  
29 2D IR spectroscopy is combined, it is possible to deduce the three-dimensional structure of a  
30 peptide assembly.<sup>72</sup> For more routine analysis, secondary structure prediction by 2D IR  
31 spectroscopy exhibits better accuracy than analysis with linear spectroscopy.<sup>73</sup>  
32

33 In addition to average structure, 2D IR spectroscopy can be used to characterize structural  
34 changes over time to advance our understanding of a variety of processes such as peptide folding  
35 and protein oligomerization.<sup>10, 74-76, 81-83</sup> For example, 2D IR spectroscopy has been extensively  
36 applied toward the study of amyloid fibril formation.<sup>77, 78</sup> Figure 7 shows 2D IR spectra from one  
37 recent study of human  $\gamma$ D-crystallin protein that employed a combination of 2D IR spectroscopy  
38 and segmental <sup>13</sup>C labeling to elucidate the involvement of the N- and C-terminal domains in the  
39 formation of amyloid fibrils.<sup>77</sup> These and similar studies take advantage of the band enhancement  
40 in the 2D spectra and the characteristic low-energy shift of the amide I mode to monitor beta sheet  
41 formation. By investigating proteins with a combination of <sup>13</sup>C-labeled N- and/or C-terminal  
42 domains, it was possible to show that the mechanism of amyloid formation depends on the route  
43 of denaturation. Comparison of the 2D spectra of the thermally induced aggregates and native  
44 states of  $\gamma$ D-crystallin labeled with <sup>13</sup>C at only the N-terminal domain (panels A and B, Fig. 7,  
45 respectively) reveals shifts to lower frequency in the amide I bands of both the <sup>13</sup>C-labeled N-  
46 terminal and unlabeled C-terminal domains (amide I bands observed at low and high frequency,  
47 respectively) that indicate beta sheet formation. In contrast, the 2D spectrum of the acid-  
48 denatured state of the N-terminally <sup>13</sup>C-labeled protein shows frequency shifts only for the high  
49 frequency, unlabeled amide bands of the C-terminal domain, not for the <sup>13</sup>C-labeled N-terminal  
50 domain (panel C, Fig. 7). Thus, the 2D IR data provide evidence that both domains of  $\gamma$ D-  
51 crystallin participate in amyloid fibril formation upon thermal denaturation, while only the C-  
52 terminal domain is involved in acid-induced fibril formation. The highly resolved structural  
53 information available from the combination of site-selective labeling and 2D IR spectroscopy  
54 should be able to yield similarly detailed insight into the molecular mechanisms underlying many  
55 biological processes.  
56

### 57 **Ligand probes**

58  
59  
60

1  
2  
3  
4  
5  
6  
7  
8  
9  
10  
11  
12  
13  
14  
15  
16  
17  
18  
19  
20  
21  
22  
23  
24  
25  
26  
27  
28  
29  
30  
31  
32  
33  
34  
35  
36  
37  
38  
39  
40  
41  
42  
43  
44  
45  
46  
47  
48  
49  
50  
51  
52  
53  
54  
55  
56  
57  
58  
59  
60

In addition to intrinsic vibrations of protein or peptide backbones, small molecule ligands can be used as reporters of their environments when bound to macromolecules. The selection of ligand reporter groups with spectrally isolated vibrational frequencies enables detection of probe absorption bands within the spectral congestion of macromolecular IR spectra. The vibrational mode of carbon monoxide bound to myoglobin was analyzed in the first demonstration of 2D IR spectroscopy to understand the dynamics of any macromolecule and has since been applied toward studying a variety of other heme proteins, such as globins and cytochromes.<sup>47, 84-89</sup> Other small molecule reporter ligands, such as nitric oxide, azide, cyanide, and azide- and nitrile-functionalized ligand analogs, permit characterization of the local binding site environment and dynamics in a wider range of proteins.<sup>31, 48, 49, 90-92</sup> 2D IR spectroscopy can be applied to measure the inhomogeneous line width that reflects the heterogeneity of a probe's local environment and, moreover, to measure spectral diffusion that reflects the dynamics among the different states, providing insight into the protein energy landscape.

For example, 2D IR spectroscopy was applied toward understanding the mechanism underlying the potency of rilpivirine, a non-nucleoside inhibitor of reverse transcriptase from human immunodeficiency virus (HIV).<sup>90</sup> Rilpivirine contains two nitrile group substituents that are required for potency, but that also fortuitously act as convenient spectrally isolated reporter vibrations for use with 2D IR spectroscopy. Upon binding reverse transcriptase and two clinically important mutant proteins, the absorption bands of the two nitrile groups become spectrally resolved, indicating that they experience distinct environments in the protein binding pocket. In addition, the observation of a fast rate of spectral diffusion suggests hydrogen bonding occurs between one of the nitriles and a mobile active site water molecule. This interaction might underlie the inhibitor's ability to retain potency against the mutants by providing an anchoring interaction that reduces the impact of other changes. As in this example, the prudent selection of reporter ligands in combination with 2D IR spectroscopy has enabled study of a wide variety of biological processes, such as protein molecular recognition, catalysis, and folding.<sup>46, 47, 86, 87, 93</sup>

### Selective side chain labeling

In principle, 2D IR spectroscopy can be applied to characterize any site in any protein by selective labeling of side chains via incorporation of unnatural amino acids functionalized with spectrally resolved vibrational probes, such as cyano (CN),<sup>50, 94-96</sup> thiocyanate (SCN),<sup>97</sup> and azido (Az)<sup>93, 98</sup> functional groups. A variety of routes exist for their site-selective incorporation into proteins. The introduction of SCN is possible by chemical modification of unique or uniquely reactive cysteine residues. Selective incorporation of cyanophenylalanine (CNPhe) and azidophenylalanine (AzPhe) is possible via the amber codon suppressor approach based on the introduction of unnatural amino acids in response to an amber (stop) codon with evolved tRNA/tRNA synthetase pairs.<sup>99</sup> Expression systems for the incorporation of both CNPhe and AzPhe have been developed.<sup>100, 101</sup> CNPhe, AzPhe, as well as a number of CN- and Az-substituted amino acids, are also available with standard protecting groups for solid phase peptide synthesis, facilitating selective incorporation via either total synthesis<sup>102</sup> or semi-synthesis with expressed protein<sup>103</sup> or native chemical ligation.<sup>104</sup>

The vibrational frequencies of these probe groups are sufficiently isolated for application to larger proteins. Unlike amide backbone modes, the vibrations of the side chain probes are largely localized to the specific probe bond(s). Their sensitivity to the electrostatic field of their local environment and short-range interactions like hydrogen bonding dominate the spectral changes, and so the probes report on their surrounding environment and dynamics when incorporated into proteins. Selection among the Az, CN, and SCN probes involves a compromise among spectral properties. The Az probe shows the most intense signals, which is advantageous for detection in nonlinear experiments of biological samples that are limited in concentration. Az groups often show Fermi resonances that complicate spectral interpretation, but the issue can be avoided with isotopic substitution.<sup>105</sup> The short vibrational lifetimes of Az groups also limit the timescale over which they can be used to measure dynamics with 2D experiments. Similarly, a trade-off between intensity and lifetime is found for different CN- and SCN-functionalized amino acids. Aromatic CN groups provide the most intense signals but show the shortest vibrational lifetimes, while

1  
2  
3  
4  
5  
6  
7  
8  
9  
10  
11  
12  
13  
14  
15  
16  
17  
18  
19  
20  
21  
22  
23  
alkyl CN groups, and even more so SCN groups, provide weaker signals but show longer vibrational lifetimes. The perturbation to the protein from incorporation of a vibrational probe should also be considered, which will depend on the specific placement of a probe within a protein, *e.g.* at a surface *vs.* interior residue.

The use of CNPhe as a probe of protein dynamics is demonstrated by several studies of a polypeptide HP35 from chicken villin protein.<sup>50, 94-96</sup> As a small system that autonomously folds into a protein-like domain, HP35 is a common subject for the study of protein folding. 2D IR spectroscopy was applied to measure folding-induced changes in dynamics reported at two CNPhe residues incorporated into HP35 via peptide synthesis (Fig. 8).<sup>50, 94</sup> Because the CNPhe vibrational frequency is highly sensitive to fluctuations in its environment, the spectral diffusion of the probe reflects the dynamics of its protein or solvent environment. For example, time-dependent 2D spectra of CNPhe in folded and guanidinium-denatured HP35 are shown in Fig. 8.<sup>50</sup> The greater elongation of the bands for the folded (upper panel, Fig. 8) compared to the unfolded state (lower panel, Fig. 8) reports on the greater heterogeneity of the environment in the folded protein compared to the homogeneous solvent environment in the unfolded state. Spectral diffusion leads to a reduction in the elongation of the 2D band shapes over time. The 2D band evolution for the folded state is demonstrably slower than for the unfolded state, which reflects the greater restriction of the dynamics in the folded state.

### Water dynamics

24  
25  
26  
27  
28  
29  
30  
31  
32  
33  
34  
35  
36  
37  
38  
39  
40  
41  
42  
43  
44  
45  
Due to its ubiquitous presence in nature, an understanding of water as a dynamic solvent could lend insight into a variety of phenomena from chemistry and biology to geology and astrophysics. 2D IR spectroscopy has been extensively applied toward advancing our fundamental understanding of water and the dynamics of its hydrogen bonding networks. A number of excellent reviews cover the work in this area.<sup>38, 106-109</sup> One longstanding question surrounds the nature of water at an interface and the potential differences from bulk water.

Water at interfaces with membranes has attracted interest due to its importance in biology and for artificial energy harvesting devices. Many studies have investigated the nature of membrane-associated water via analysis of O-H or O-D stretching vibrations to directly probe water structure and dynamics.<sup>42, 110, 111</sup> Another approach is to characterize the dynamics of interfacial water molecules via their influence on the spectral dynamics of another probe group, such as the phosphate head groups of the constituent lipids or small molecules added to membranes.<sup>112, 113</sup> Reverse micelles serve as a useful model system for investigating the differences between bulk and interfacial water, as their preparation with defined size is well established and enables control over the proportion of water in the bulk “nanopool” or at the interface.<sup>42, 110, 111</sup> Measurement of the spectral diffusion for water in the two populations with 2D IR spectroscopy shows that the dynamics of interfacial water molecules exhibit markedly slower dynamics than those in bulk solution. Additional 2D IR studies of different membrane structures, such as bicelles and lipid bilayers<sup>112, 113</sup> find water dynamics at the interface are generally slower than in bulk solution, supporting the idea that the presence of an interface can impact the nature of water and potentially its behavior in chemical and biological systems.

In addition to membranes, 2D IR spectroscopy has been used to probe water dynamics at the interface with DNA<sup>68</sup> and proteins/peptides.<sup>43, 114-119</sup> Both the O-H stretching vibration of the surrounding water and the N-H vibrations of the nucleotide bases have been used to measure the dynamics of the water shell around DNA oligomers. The hydration layer of proteins can be characterized via the attachment of vibrational probe groups that are sensitive to the dynamics of surrounding water.<sup>114, 117</sup> For example, site-selective labeling of lysozyme with a ruthenium carbonyl complex and characterization of the vibrational spectral diffusion with 2D IR spectroscopy permitted measurement of water dynamics within its hydration shell (Fig. 9).<sup>114</sup> As observed in studies of membrane-associated water, water at the surface of the protein exhibits markedly slower dynamics than the bulk. Interestingly, the study of lysozyme found that water associated with structured regions of the protein show slower dynamics, while water associated with unstructured, more flexible regions appear to maintain bulk-like behavior.<sup>115</sup>

1  
2  
3  
4 Another approach to characterize protein-associated water is via the influence of water on  
5 spectral dynamics of  $^{13}\text{C}/^{18}\text{O}$ -shifted vibrations of selectively labeled backbone amide modes.<sup>116,</sup>  
6 <sup>118, 119</sup> For example, the dynamics of water in the M2 proton channel from the influenza A virus  
7 have been characterized in this manner and related to pH-dependent conformational changes.<sup>118</sup>  
8 Perturbation of the ordered water within the channel is observed upon binding of drug molecules,  
9 providing molecular insight into the potential entropic gain underlying the favorability of  
10 binding.<sup>119</sup> These and other studies suggest that the dynamics of protein-associated water are  
11 heterogeneous, and that the nature of these dynamics might be important to protein function. The  
12 information that can be gained with 2D IR spectroscopy can provide valuable insight into the role  
13 water plays in a variety of complex biological settings and processes.

### 14 **Applications in materials chemistry**

15 In addition to the associated water at the membrane interface, 2D IR spectroscopy can yield  
16 insight into interior membrane structure and dynamics.<sup>51, 52, 113, 120</sup> The use of nonpolar molecules  
17 as vibrational probes permits selective measurement of the spectral dynamics due to fluctuations  
18 within the interior hydrophobic bilayer environment.<sup>51, 113</sup> For example, recent experiments took  
19 advantage of the intense absorption bands of the small, nonpolar molecular probe tungsten  
20 hexacarbonyl to measure the dynamics of both planar and vesicular bilayers with 2D IR  
21 spectroscopy. Large changes in structural dynamics occur upon bilayer phase transitions induced  
22 by dehydration or cholesterol addition, and furthermore, the changes are influenced by the degree  
23 of bilayer curvature.<sup>51, 52, 120</sup> The combination of similar probes with 2D IR spectroscopy could  
24 advance our understanding of membrane biophysics and potentially how variations in membrane  
25 properties due to lipid or protein composition might influence biological systems.

26 The characterization of materials important for such uses as heterogeneous catalysis, fuel cells,  
27 and molecular electronics is another interesting application of 2D IR spectroscopy.<sup>44, 121-123</sup> For  
28 instance, polymer thin films of varying conductivity have been investigated using embedded  
29 metal-carbonyl complex reporter molecules.<sup>121</sup> The measurement of spectral diffusion for this  
30 system provides evidence that structural dynamics in addition to the static structure contribute to  
31 the conductivity of the thin films. The interface with materials can also critically influence  
32 chemical behavior, in particular in heterogeneous catalysis. To investigate such systems, 2D IR  
33 spectroscopy has been performed on a monolayer of a Re-carbonyl complex covalently attached  
34 via a linker to a silica surface, of interest due to the potential of this and similar systems as  
35 photoreduction catalysts (Fig. 10).<sup>122</sup> The spectral diffusion of the carbonyl vibrations reflects the  
36 dynamics of the catalyst and how they are influenced by factors such as solvation, surface density,  
37 and linker length. Other studies directed at a similar Re-carbonyl complex-based catalyst, but  
38 containing a different linker attachment to a  $\text{TiO}_2$  surface, found the spectral diffusion to depend  
39 on the surface density of the catalyst, indicating coupling between molecules even at low surface  
40 densities.<sup>44</sup> Because the interfacial heterogeneity and intermolecular interactions can influence the  
41 performance of photocatalytic devices, for instance by contributing to energy relaxation pathways  
42 that compete with charge transport, understanding their structure and dynamics with 2D IR  
43 spectroscopy should be valuable for their future optimization.

44 Other studies have shown the utility of 2D IR spectroscopy for characterization of  
45 nanomaterial surfaces. For example, the three-dimensional molecular conformations of capping  
46 molecules on gold nanoparticles have been deduced via structural constraints determined from  
47 cross-band intensities in polarization-dependent 2D IR spectra.<sup>124</sup> This achievement relied on  
48 measurement of cross-band anisotropy, as well as the dependence of the coupling strength on the  
49 proximity and relative orientation of the capping molecules, similar in principle to the previously  
50 mentioned experiments for determining peptide structure. Finally, an exciting new development  
51 is the demonstration of surface-enhanced 2D IR signals, recently observed for vibrational modes  
52 of capping ligands on gold nanoparticles.<sup>125</sup> Nearly 100-fold signal enhancements promise  
53 increased sensitivity in 2D IR spectroscopy for sensor and other applications demanding dilute or  
54 weakly absorbing samples. Such surface-enhanced 2D methods could find wide-ranging  
55 applications in analytical chemistry similar to linear surface-enhanced Raman and IR  
56 spectroscopy.  
57  
58  
59  
60

## Summary and outlook.

2D IR spectroscopy is a powerful approach to the analysis of molecular structure and dynamics on fast timescales with bond-specific spatial resolution. The additional information provided by the second dimension, as well as the versatility in temporal and polarization control of pulses, facilitate spectral assignment and interpretation, which is particularly critical to studies of complex molecules. We briefly highlighted a few examples that illustrate the potential applications of 2D IR spectroscopy to address chemical and biological questions. 2D IR spectroscopy of nucleic acid systems is yet to be fully developed. Particularly exciting is the further extension of the methods to understand the biophysics of RNA, highly flexible biomolecules with dynamics likely critical to their function, but difficult to study with traditional methods. Although the application of 2D IR spectroscopy to study the biophysics of peptides and proteins is more developed, the scope of the methods has yet to be fully explored. The combination of 2D IR spectroscopy with site-selective labeling with vibrational probes promises to emerge as a particularly powerful approach for the study of side chain dynamics, which are believed to contribute critically to protein function on fast timescales.<sup>126-128</sup> Only a handful of proteins thus far have been analyzed via this route. The incorporation of multiple probes in one protein and the potential to obtain distance and orientation information from their coupling, as is currently performed with the <sup>13</sup>C/<sup>18</sup>O-labeled backbone of peptides, is a future possibility. This approach will benefit from further development of spectrally resolved vibrational probes with more intense signals and longer lifetimes, as well as chemical and biological methods for their site-selective incorporation into proteins and nucleic acids.

Only the basic experimental implementation of 2D IR spectroscopy was presented in this minireview. A wide variety of extensions on this experiment have been developed.<sup>9-18</sup> For instance, transient 2D IR spectroscopy is possible when combined with laser-induced temperature jump, photo-induced isomerization, or rapid mixing to initiate chemical reactions.<sup>10, 71, 76, 81-83, 129</sup> Multidimensional experiments involving a combination of visible and IR excitation beams also have been reported,<sup>130, 131</sup> providing information about vibronic coupling that promises to be particularly powerful for advancing our understanding of photosynthetic systems. Frequency-domain versions of 2D IR and visible-IR nonlinear experiments based on Raman processes, which employ narrow band, tunable excitation pulses, have also been well developed and applied in a variety of studies, for example in both nanomaterial and proteomic research.<sup>21, 132, 133</sup> In addition, several groups have performed 2D IR experiments using ultra-broadband probe pulses.<sup>13, 134-136</sup> Such broadband detection will facilitate analysis of chemical samples with features encompassing wide spectral ranges. Recently, 2D IR spectroscopy was implemented in attenuated total reflection mode,<sup>137</sup> which has long been used in linear spectroscopy for its selective sensitivity to molecules at the prism surface. Experiments performed in reflection mode could find wide application in materials science. Finally, the large signal enhancements possible using surface-enhanced 2D IR spectroscopy could significantly improve levels of detection and widely extend the application of 2D IR spectroscopy in the analytical sciences.<sup>125</sup> Overall, the rich toolbox of multidimensional IR methods provides a versatile route for characterization of a variety of different samples and for addressing a wide range of scientific questions.

## Acknowledgements

The authors would like to thank Indiana University and the Department of Energy (DE-FOA-0000751) for funding. R. H. was also supported by the Graduate Training Program in Quantitative and Chemical Biology (T32 GM109825).

## Notes and references

1. J. Zheng, K. Kwak and M. D. Fayer, *Acc. Chem. Res.*, 2007, **40**, 75-83.
2. S. Park, K. Kwak and M. D. Fayer, *Laser Phys. Lett.*, 2007, **4**, 704-718.

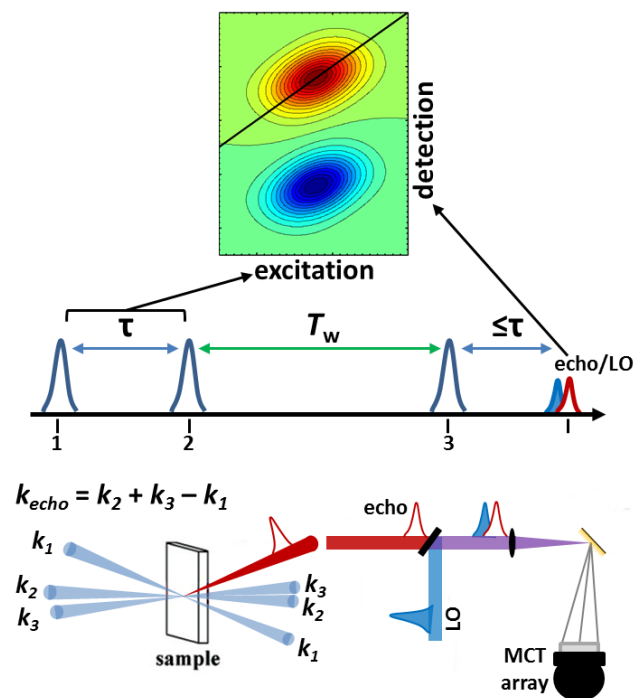
3. R. M. Hochstrasser, *Proc. Natl. Acad. Sci. U. S. A.*, 2007, **104**, 14190-14196.
4. S. Mukamel, *Principles of Nonlinear Optics and Spectroscopy*, Oxford University Press, New York, 1995.
5. P. Hamm and M. Zanni, *Concepts and Methods of 2D Infrared Spectroscopy*, Cambridge University Press, 2011.
6. M. Cho, *Two-Dimensional Optical Spectroscopy*, CRC Press, Boca Raton, 2009.
7. M. D. Fayer, *Ultrafast Infrared Vibrational Spectroscopy*, CRC Press, Boca Raton, 2013.
8. M. Cho, *Chem. Rev.*, 2008, **108**, 1331-1418.
9. D. B. Strasfeld, S. H. Shim and M. Zanni, in *Advances in Chemical Physics*, ed. S. A. Rice, John Wiley and Sons, Inc., Hoboken, New Jersey, 2009, vol. 141, pp. 1-28.
10. M. J. Tucker, M. Abdo, J. R. Courter, J. Chen, S. P. Brown, A. B. Smith, 3rd and R. M. Hochstrasser, *Proc. Natl. Acad. Sci. U. S. A.*, 2013, **110**, 17314-17319.
11. M. Khalil, N. Demirdoven and A. Tokmakoff, *J. Phys. Chem. A*, 2003, **107**, 5258-5279.
12. R. M. Hochstrasser, *Chem. Phys.*, 2001, **266**, 273-284.
13. C. R. Baiz and K. J. Kubarych, *Opt. Lett.*, 2011, **36**, 187-189.
14. M. J. Nee, R. McCanne and K. J. Kubarych, *Opt. Lett.*, 2007, **32**, 713-715.
15. M. F. DeCamp, L. P. DeFlores, K. C. Jones and A. Tokmakoff, *Opt. Express*, 2007, **15**, 233-241.
16. L. P. DeFlores, R. A. Nicodemus and A. Tokmakoff, *Opt. Lett.*, 2007, **32**, 2966-2968.
17. S. S. Mukherjee, D. R. Skoff, C. T. Middleton and M. T. Zanni, *J. Chem. Phys.*, 2013, **139**, 144205.
18. J. Helbing and P. Hamm, *J. Opt. Soc. Am. B*, 2011, **28**, 171-178.
19. J. C. Wright, *Annu. Rev. Phys. Chem.*, 2011, **62**, 209-230.
20. E. S. Boyle, N. A. Neff-Mallon and J. C. Wright, *J. Phys. Chem. A*, 2013, **117**, 12401-12408.
21. F.ournier, R. Guo, E. M. Gardner, P. M. Donaldson, C. Loeffeld, I. R. Gould, K. R. Willison and D. R. Klug, *Acc. Chem. Res.*, 2009, **42**, 1322-1331.
22. V. Cervetto, J. Helbing, J. Bredenbeck and P. Hamm, *J. Chem. Phys.*, 2004, **121**, 5935-5942.
23. S. H. Shim, D. B. Strasfeld and M. Zanni, *Opt. Express*, 2006, **14**, 13120-13130.
24. PhaseTech Spectroscopy, <http://phasetechspectroscopy.com>, (accessed March 19, 2015).
25. M. Zanni, in *Ultrafast Phenomena*, eds. P. Corkum, S. de Silvestri, K. A. Nelson, E. Reidle and R. W. Schoenlein, Springer, Berlin, 2009, vol. 92, pp. 397-399.
26. S. K. K. Kumar, A. Tamimi and M. D. Fayer, *J. Chem. Phys.*, 2012, **137**, 184201.
27. W. Rock, Y. L. Li, P. Pagano and C. M. Cheatum, *J. Phys. Chem. A*, 2013, **117**, 6073-6083.
28. K. H. Park, S. R. Choi, J.-H. Choi, S. Park and M. Cho, *ChemPhysChem*, 2010, **11**, 3632-3637.
29. J. F. Brookes, K. M. Slenkamp, M. S. Lynch and M. Khalil, *J. Phys. Chem. A*, 2013, **117**, 6234-6243.
30. N. Simpson, D. J. Shaw, P. W. J. M. Frederix, A. H. Gillies, K. Adamczyk, G. M. Greetham, M. Towrie, A. W. Parker, P. A. Hoskisson and N. T. Hunt, *J. Phys. Chem. B*, 2013, **117**, 16468-16478.
31. S. Dutta, Y.-L. Li, W. Rock, J. C. D. Houtman, A. Kohen and C. M. Cheatum, *J. Phys. Chem. B*, 2012, **116**, 542-548.
32. M. J. Tucker, X. S. Gai, E. E. Fenlon, S. H. Brewer and R. M. Hochstrasser, *Phys. Chem. Chem. Phys.*, 2011, **13**, 2237-2241.
33. H. Kim and M. Cho, *Chem. Rev.*, 2013, **113**, 5817-5847.
34. M. R. Panman, J. Vos, V. Bocokic, R. Bellini, B. de Bruin, J. H. N. Reek and S. Woutersen, *Inorg. Chem.*, 2013, **52**, 14294-14298.
35. A. T. Messmer, K. M. Lippert, P. R. Schreiner and J. Bredenbeck, *Phys. Chem. Chem. Phys.*, 2013, **15**, 1509-1517.
36. Z. Sun, W. Zhang, M. Ji, R. Hartsock and K. J. Gaffney, *J. Phys. Chem. B*, 2013, **117**, 12268-12275.
37. H. Bian, H. Chen, Q. Zhang, J. Li, X. Wen, W. Zhuang and J. Zheng, *J. Phys. Chem. B*, 2013, **117**, 7972-7984.
38. M. D. Fayer, *Acc. Chem. Res.*, 2012, **45**, 3-14.
39. D. G. Kuroda and R. M. Hochstrasser, *Phys. Chem. Chem. Phys.*, 2012, **14**, 6219-6224.
40. A. Huerta-Viga, S. R. Domingos, S. Amirjalayer and S. Woutersen, *Phys. Chem. Chem. Phys.*, 2014, **16**, 15784-15786.
41. K. Kwak, S. Park, I. J. Finkelstein and M. D. Fayer, *J. Chem. Phys.*, 2007, **127**, 124503.
42. E. E. Fenn, D. B. Wong, C. H. Giammanco and M. D. Fayer, *J. Phys. Chem. B*, 2011, **115**, 11658-11670.
43. A. C. Fogarty and D. Laage, *J. Phys. Chem. B*, 2014, **118**, 7715-7729.
44. J. E. Laaser, J. R. Christianson, T. A. Oudenhoven, Y. Joo, P. Gopalan, J. R. Schmidt and M. T. Zanni, *J. Phys. Chem. C*, 2014, **118**, 5854-5861.
45. J. T. King and K. J. Kubarych, *J. Am. Chem. Soc.*, 2012, **134**, 18705-18712.
46. I. J. Finkelstein, H. Ishikawa, S. Kim, A. M. Massari and M. D. Fayer, *Proc. Natl. Acad. Sci. U. S. A.*, 2007, **104**, 2637-2642.
47. M. C. Thielges and M. D. Fayer, *Acc. Chem. Res.*, 2012, **45**, 1866-1874.
48. J. N. Bandaria, S. Dutta, M. W. Nydegger, W. Rock, A. Kohen and C. M. Cheatum, *Proc. Natl. Acad. Sci. U. S. A.*, 2010, **107**, 17974-17979.
49. M. Cheng, J. F. Brookes, W. R. Montfort and M. Khalil, *J. Phys. Chem. B*, 2013, **117**, 15804-15811.
50. J. K. Chung, M. C. Thielges and M. D. Fayer, *Proc. Natl. Acad. Sci. U. S. A.*, 2011, **108**, 3578-3583.
51. O. Kel, A. Tamimi and M. D. Fayer, *Proc. Natl. Acad. Sci. U. S. A.*, 2014, **111**, 918-923.
52. S. K. K. Kumar, A. Tamimi and M. D. Fayer, *J. Am. Chem. Soc.*, 2013, **135**, 5118-5126.
53. A. D. Hill, M. C. Zorb, S. C. Nguyen, J. P. Lomont, M. A. Bowring and C. B. Harris, *J. Phys. Chem. B*, 2013, **117**, 15346-15355.
54. D. V. Kurochkin, S. R. G. Naraharisetty and I. V. Rubtsov, *Proc. Natl. Acad. Sci. U. S. A.*, 2007, **104**, 14209-14214.
55. Z. Lin and I. V. Rubtsov, *Proc. Natl. Acad. Sci. U. S. A.*, 2012, **109**, 1413-1418.
56. H. Chen, X. Wen, J. Li and J. Zheng, *J. Phys. Chem. A*, 2014, **118**, 2463-2469.
57. C. S. Peng, K. C. Jones and A. Tokmakoff, *J. Am. Chem. Soc.*, 2011, **133**, 15650-15660.
58. C. Greve, N. K. Preketes, H. Fidler, R. Costard, B. Koeppe, I. A. Heisler, S. Mukamel, F. Temps, E. T. J. Nibbering and T. Elsaesser, *J. Phys. Chem. A*, 2013, **117**, 594-606.
59. C. Greve, N. K. Preketes, R. Costard, B. Koeppe, H. Fidler, E. T. J. Nibbering, F. Temps, S. Mukamel and T. Elsaesser, *J. Phys. Chem. A*, 2012, **116**, 7636-7644.

- 1  
2  
3  
4  
5  
6  
7  
8  
9  
10  
11  
12  
13  
14  
15  
16  
17  
18  
19  
20  
21  
22  
23  
24  
25  
26  
27  
28  
29  
30  
31  
32  
33  
34  
35  
36  
37  
38  
39  
40  
41  
42  
43  
44  
45  
46  
47  
48  
49  
50  
51  
52  
53  
54  
55  
56  
57  
58  
59  
60
60. C. Greve and T. Elsaesser, *J. Phys. Chem. B*, 2013, **117**, 14009-14017.  
61. M. Yang, L. Szyz and T. Elsaesser, *J. Phys. Chem. B*, 2011, **115**, 1262-1267.  
62. A. T. Krummel, P. Mukherjee and M. T. Zanni, *J. Phys. Chem. B*, 2003, **107**, 9165-9169.  
63. A. T. Krummel and M. T. Zanni, *J. Phys. Chem. B*, 2006, **110**, 13991-14000.  
64. M. Yang, L. Szyz, K. Rottger, H. Fidder, E. T. J. Nibbering, T. Elsaesser and F. Temps, *J. Phys. Chem. B*, 2011, **115**, 5484-5492.  
65. H. Fidder, M. Yang, E. T. J. Nibbering, T. Elsaesser, K. Rottger and F. Temps, *J. Phys. Chem. A*, 2013, **117**, 845-854.  
66. C. Lee, K. H. Park and M. Cho, *J. Chem. Phys.*, 2006, **125**, 114508.  
67. C. Lee and M. Cho, *J. Chem. Phys.*, 2006, **125**, 114509.  
68. M. Yang, L. Szyz and T. Elsaesser, *J. Phys. Chem. B*, 2011, **115**, 13093-13100.  
69. V. Singh, C. S. Peng, D. Li, K. Mitra, K. J. Silvestre, A. Tokmakoff and J. M. Essigmann, *ACS Chem. Biol.*, 2014, **9**, 227-236.  
70. C. S. Peng and A. Tokmakoff, *J. Phys. Chem. Lett.*, 2012, **3**, 3302-3306.  
71. C. S. Peng, C. R. Baiz and A. Tokmakoff, *Proc. Natl. Acad. Sci. U. S. A.*, 2013, **110**, 9243-9248.  
72. A. Remorino, I. V. Korendovych, Y. Wu, W. F. DeGrado and R. M. Hochstrasser, *Science*, 2011, **332**, 1206-1209.  
73. C. R. Baiz, C. S. Peng, M. E. Reppert, K. C. Jones and A. Tokmakoff, *Analyst*, 2012, **137**, 1793-1799.  
74. Z. Ganim, K. C. Jones and A. Tokmakoff, *Phys. Chem. Chem. Phys.*, 2012, **12**, 3579-3588.  
75. H. Maekawa, M. De Poli, C. Toniolo and N.-H. Ge, *J. Am. Chem. Soc.*, 2009, **131**, 2042-2043.  
76. K. C. Jones, C. S. Peng and A. Tokmakoff, *Proc. Natl. Acad. Sci. U. S. A.*, 2013, **110**, 2828-2833.  
77. S. D. Moran, T. O. Zhang and M. T. Zanni, *Protein Sci*, 2014, **23**, 321-331.  
78. S. D. Moran, A. M. Woys, L. E. Buchanan, E. Bixby, S. M. Decatur and M. T. Zanni, *Proc. Natl. Acad. Sci. U. S. A.*, 2012, **109**, 3329-3334.  
79. L. E. Buchanan, E. B. Dunkelberger, H. Q. Tran, P.-N. Cheng, C.-C. Chiu, P. Cao, D. P. Raleigh, J. J. de Pablo, J. S. Nowick and M. T. Zanni, *Proc. Natl. Acad. Sci. U. S. A.*, 2013, **110**, 19285-19290.  
80. M. Grechko and M. T. Zanni, *J. Chem. Phys.*, 2012, **137**, 184202.  
81. H. S. Chung, Z. Ganim, K. C. Jones and A. Tokmakoff, *Proc. Natl. Acad. Sci. U. S. A.*, 2007, **104**, 14237-14342.  
82. P. Hamm, J. Helbing and J. Bredenbeck, *Annu. Rev. Phys. Chem.*, 2008, **59**, 291-317.  
83. M. J. Tucker, M. Abdo, J. R. Courter, J. Chen, A. B. Smith, 3rd and R. M. Hochstrasser, *J. Photochem. Photobiol. A*, 2012, **234**, 156-163.  
84. K. A. Merchant, D. E. Thompson, Q.-H. Xu, R. B. Williams, R. F. Loring and M. D. Fayer, *Biophys. J.*, 2002, **82**, 3277-3288.  
85. M. C. Thielges, J. K. Chung and M. D. Fayer, *J. Am. Chem. Soc.*, 2011, **133**, 3995-4004.  
86. J. K. Chung, M. C. Thielges, S. E. J. Bowman, K. L. Bren and M. D. Fayer, *J. Am. Chem. Soc.*, 2011, **133**, 6681-6691.  
87. H. Ishikawa, K. Kwak, J. K. Chung, S. Kim and M. D. Fayer, *Proc. Natl. Acad. Sci. U. S. A.*, 2008, **105**, 8619-8624.  
88. H. Ishikawa, I. J. Finkelstein, S. Kim, K. Kwak, J. K. Chung, K. Wakasugi, A. M. Massari and M. D. Fayer, *Proc. Natl. Acad. Sci. U. S. A.*, 2007, **104**, 16116-16121.  
89. I. J. Finkelstein, J. Zheng, H. Ishikawa, S. Kim, K. Kwak and M. D. Fayer, *Phys. Chem. Chem. Phys.*, 2007, **9**, 1533-1549.  
90. D. G. Kuroda, J. D. Bauman, J. R. Challa, D. Patel, T. Troxler, K. Das, E. Arnold and R. M. Hochstrasser, *Nat. Chem.*, 2013, **5**, 174-181.  
91. K. Adamczyk, M. Candelaesi, R. Kania, K. Robb, C. Bellota-Anton, G. M. Greetham, M. R. Pollard, M. Towrie, A. W. Parker, P. A. Hoskisson, N. P. Tucker and N. T. Hunt, *Phys. Chem. Chem. Phys.*, 2012, **14**, 7411-7419.  
92. M. Maj, Y. Oh, K. Park, J. Lee, K. W. Kwak and M. Cho, *J. Chem. Phys.*, 2014, **140**, 235104.  
93. R. Bloem, K. Koziol, S. A. Waldauer, B. Buchli, R. Wälsler, B. Samatanga, I. Jelesarov and P. Hamm, *J. Phys. Chem. B*, 2012, **116**, 13705-13712.  
94. J. K. Chung, M. C. Thielges and M. D. Fayer, *J. Am. Chem. Soc.*, 2012, **134**, 12118-12124.  
95. D. C. Urbanek, D. Y. Vorobyev, A. L. Serrano, F. Gai and R. M. Hochstrasser, *J. Phys. Chem. Lett.*, 2010, **1**, 3311-3315.  
96. S. Bagchi, S. G. Boxer and M. D. Fayer, *J. Phys. Chem. B*, 2012, **116**, 4034-4042.  
97. L. J. G. W. van Wilderen, D. Kern-Michler, H. M. Muller-Werkmeister and J. Bredenbeck, *Phys. Chem. Chem. Phys.*, 2014, **16**, 19643-19653.  
98. M. C. Thielges, J. Y. Axup, D. Wong, H. S. Lee, J. K. Chung, P. G. Schultz and M. D. Fayer, *J. Phys. Chem. B*, 2011, **115**, 11294-11304.  
99. C. C. Liu and P. G. Schultz, *Annu. Rev. Biochem.*, 2010, **79**, 413-444.  
100. K. C. Schultz, L. Supekova, Y. Ryu, J. Xie, R. Perera and P. G. Schultz, *J. Am. Chem. Soc.*, 2006, **128**, 13984-13985.  
101. S. Ohno, T. Yokogawa and K. Nishikawa, *J. Biochem.*, 2001, **130**, 417-423.  
102. P. E. Dawson, M. C. Fitzgerald, T. W. Muir and S. B. H. Kent, *J. Am. Chem. Soc.*, 1997, **119**, 7917-7927.  
103. T. W. Muir, *Annu. Rev. Biochem.*, 2003, **72**, 249-289.  
104. P. E. Dawson and S. B. H. Kent, *Annu. Rev. Biochem.*, 2000, **69**, 923-960.  
105. J. S. Lipkin, R. Song, E. F. Fenlon and S. H. Brewer, *J. Phys. Chem. Lett.*, 2011, **2**, 1672-1676.  
106. D. Laage, G. Stirnemann, F. Sterpone and J. T. Hynes, *Acc. Chem. Res.*, 2012, **45**, 53-62.  
107. S. T. Roberts, K. Ramasesha and A. Tokmakoff, *Acc. Chem. Res.*, 2009, **42**, 1239-1249.  
108. H. J. Bakker and J. L. Skinner, *Chem. Rev.*, 2010, **110**, 1498-1517.  
109. M. D. Fayer, D. E. Moilanen, D. Wong, D. E. Rosenfeld, E. E. Fenn and S. Park, *Acc. Chem. Res.*, 2009, **42**, 1210-1219.  
110. A. A. Bakulin, D. Cringus, P. A. Pieniazek, J. L. Skinner, T. L. C. Jansen and M. S. Pshenichnikov, *J. Phys. Chem. B*, 2013, **117**, 15545-15558.  
111. R. Costard, C. Greve, I. A. Heisler and T. Elsaesser, *J. Phys. Chem. Lett.*, 2012, **3**, 3646-3651.  
112. R. Costard, I. A. Heisler and T. Elsaesser, *J. Phys. Chem. Lett.*, 2014, **5**, 506-511.  
113. D. G. Osborne, J. A. Dunbar, J. G. Lapping, A. M. White and K. J. Kubarych, *J. Phys. Chem. B*, 2013, **117**, 15407-15414.  
114. J. T. King, E. J. Arthur, C. L. Brooks, 3rd and K. J. Kubarych, *J. Am. Chem. Soc.*, 2014, **136**, 188-194.  
115. J. T. King, E. J. Arthur, C. L. Brooks, 3rd and K. J. Kubarych, *J. Phys. Chem. B*, 2012, **116**, 5604-5611.  
116. A. Ghosh and R. M. Hochstrasser, *Chem. Phys.*, 2011, **390**, 1-13.

- 1  
2  
3  
4  
5  
6  
7  
8  
9  
10  
11  
12  
13  
14  
15  
16  
17  
18  
19  
20  
21  
22  
23  
24  
25  
26  
27  
28  
29  
30  
31  
32  
33  
34  
35  
36  
37  
38  
39  
40  
41  
42  
43  
44  
45  
46  
47  
48  
49  
50  
51  
52  
53  
54  
55  
56  
57  
58  
59  
60
117. A. M. Woys, S. S. Mukherjee, D. R. Skoff, S. D. Moran and M. T. Zanni, *J. Phys. Chem. B*, 2013, **117**, 5009-5018.  
 118. A. Ghosh, J. Qiu, W. F. DeGrado and R. M. Hochstrasser, *Proc. Natl. Acad. Sci. U. S. A.*, 2011, **108**, 6115-6120.  
 119. A. Ghosh, J. Wang, Y. S. Moroz, I. V. Korendovych, M. Zanni, W. F. DeGrado, F. Gai and R. M. Hochstrasser, *J. Chem. Phys.*, 2014, **140**, 235105.  
 120. O. Kel, A. Tamimi and M. D. Fayer, *J. Phys. Chem. B*, 2014. DOI: 10.1021/jp503940k.  
 121. A. A. Eigner, B. H. Jones, B. W. Koprucki and A. M. Massari, *J. Phys. Chem. B*, 2011, **115**, 4583-4591.  
 122. D. E. Rosenfeld, Z. Gengeliczki, B. J. Smith, T. D. Stack and M. D. Fayer, *Science*, 2011, **334**, 634-639.  
 123. D. E. Rosenfeld, J. Nishida, C. Yan, Z. Gengeliczki, B. J. Smith and M. D. Fayer, *J. Phys. Chem. C*, 2012, **116**, 23428-23440.  
 124. H. Bian, J. Li, H. Chen, K. Yuan, X. Wen, Y. Li, Z. Sun and J. Zheng, *J. Phys. Chem. C*, 2012, **116**, 7913-7924.  
 125. P. M. Donaldson and P. Hamm, *Angew. Chem. Int. Ed. Engl.*, 2013, **52**, 634-638.  
 126. K. Henzler-Wildman and D. Kern, *Nature*, 2007, **450**, 964-972.  
 127. V. A. Jarmowycz and M. J. Stone, *Chem. Rev.*, 2006, **106**, 1624-1671.  
 128. M. S. Marlow, J. Dogan, K. K. Frederick, K. G. Valentine and A. J. Wand, *Nat. Chem. Biol.*, 2010, **6**, 352-358.  
 129. V. Cervetto, P. Hamm and J. Helbing, *J. Phys. Chem. B*, 2008, **112**, 8398-8405.  
 130. T. A. A. Oliver, N. H. C. Lewis and G. R. Fleming, *Proc. Natl. Acad. Sci. U. S. A.*, 2014, **111**, 10061-10066.  
 131. P. M. Donaldson, H. Strzalka and P. Hamm, *Opt. Express*, 2012, **20**, 12761-12770.  
 132. F. Fournier, E. M. Gardner, D. A. Kedra, P. M. Donaldson, R. Guo, S. A. Butcher, I. R. Gould, K. R. Willison and D. R. Klug, *Proc. Natl. Acad. Sci. U. S. A.*, 2008, **105**, 15352-15357.  
 133. A. V. Pakoulev, M. A. Rickard, K. M. Kornau, N. A. Mathew, L. A. Yurs, S. B. Block and J. A. Wright, *Acc. Chem. Res.*, 2009, **42**, 1310-1321.  
 134. A. M. Stingel, C. Calabrese and P. B. Petersen, *J. Phys. Chem. B*, 2013, **117**, 15714-15719.  
 135. L. De Marco, K. Ramasesha and A. Tokmakoff, *J. Phys. Chem. B*, 2013, **117**, 15319-15327.  
 136. M. Cheng, A. Reynolds, H. Widgren and M. Khalil, *Opt. Lett.*, 2012, **37**, 1787-1789.  
 137. J. P. Kraack, D. Lotti and P. Hamm, *J. Phys. Chem. Lett.*, 2014, **5**, 2325-2329.

## Figures.

Figure 1. Simulated example 2D IR spectra and schematic illustrating 2D IR experimental pulse timing, geometry, and detection. Adapted with permission from Zheng *et al.* *Accounts of Chemical Research*, 2007, **40**, 75-83. Copyright © 2007 American Chemical Society.



1  
2  
3  
4  
5  
6  
7  
8  
9  
10  
11  
12  
13  
14  
15  
16  
17  
18  
19  
20  
21  
22  
23  
24  
25  
26  
27  
28  
29  
30  
31  
32  
33  
34  
35  
36  
37  
38  
39  
40  
41  
42  
43  
44  
45  
46  
47  
48  
49  
50  
51  
52  
53  
54  
55  
56  
57  
58  
59  
60

Figure 2. Polarization-dependent 2D IR spectra of an equimolar solution of Diels Alder substrate *N*-crotonyloxazolidinone and catalyst  $\text{SnCl}_4$  (see text). Each of the red and green gridlines indicate bands due to a single species. The FTIR spectra are shown above the left panel for the mixture (black), the substrate (green), and the catalyst (red). The structures of the *syn* conformer of the substrate-catalyst complex and the *anti* conformer of the substrate are shown below. Adapted from Ref. 35 with permission from the PCCP Owner Societies.

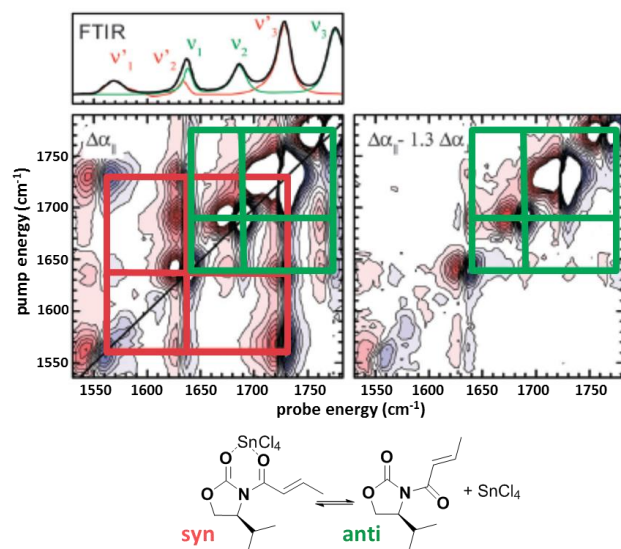


Figure 3. 2D IR spectra of a solution of  $\text{NaNCS}$  and  $\text{MgI}_2$  at several waiting times. Reprinted with permission from Sun *et al.* *The Journal of Physical Chemistry B*, 2013, **117**, 12268 – 12275. Copyright © 2013 American Chemical Society.

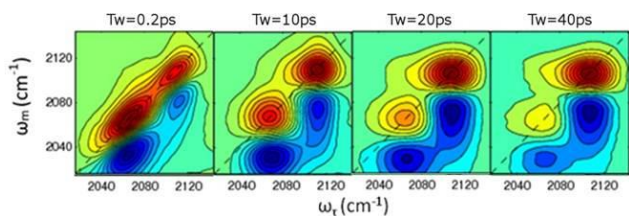


Figure 4. 2D IR spectra of solutions of sodium nitroprusside in ethylene glycol (upper panels) and water (lower panels) at several waiting times. Adapted with permission from Brookes *et al. The Journal of Physical Chemistry A*, 2013, **117**, 6234 – 6243. Copyright © 2013 American Chemical Society.

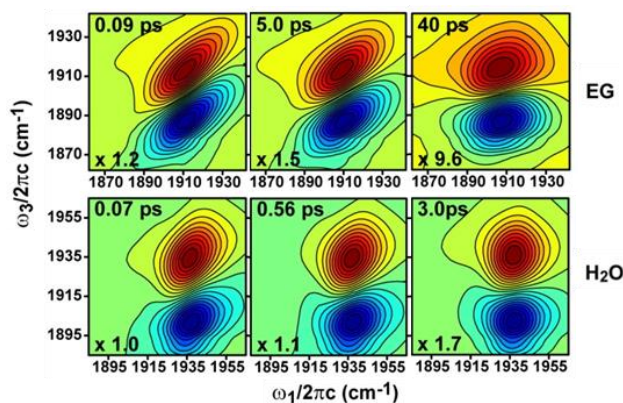


Figure 5. Structure and 2D IR spectrum of PEG<sub>4</sub> with azido and succinimide ester reporter labels ( $T_w$  of 60 ps). To the left and above the axes of the 2D spectrum are the FTIR spectra of the labeled PEG<sub>4</sub> molecule (blue) and spectra of the laser pulses (green) used to pump and probe the molecule, respectively. Reprinted with permission from Lin, Z. and Rubtsov, I.V. *Proceedings of the National Academy of Sciences of the United States of America*, 2012, **109**, 1413 – 1418.

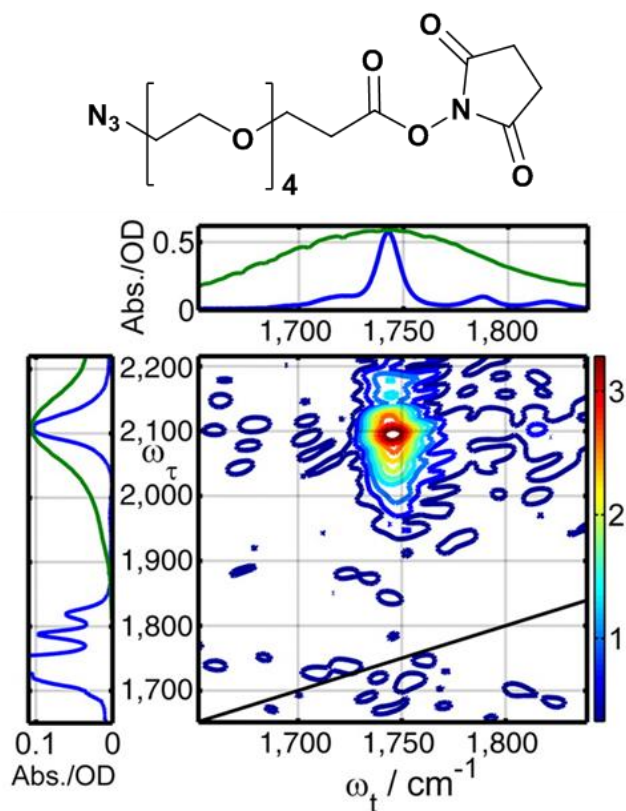


Figure 6. FTIR spectra of oxythiamine taken at various temperatures (upper panel) and 2D IR spectrum taken at 10 °C (lower panel). Blue and green lines in the 2D spectrum are shown along the frequencies of the carbonyl modes of the two keto tautomers (X1a and X1b). The presence of a cross-band between a mode associated with a methyl vibration (X4) at 1525 cm<sup>-1</sup> and the X1a mode, and the absence of one with the X1b, is highlighted with a red ellipse. Reprinted with permission from Singh *et al.* *ACS Chemical Biology*, 2014, **9**, 227 - 236. Copyright © 2014 American Chemical Society.

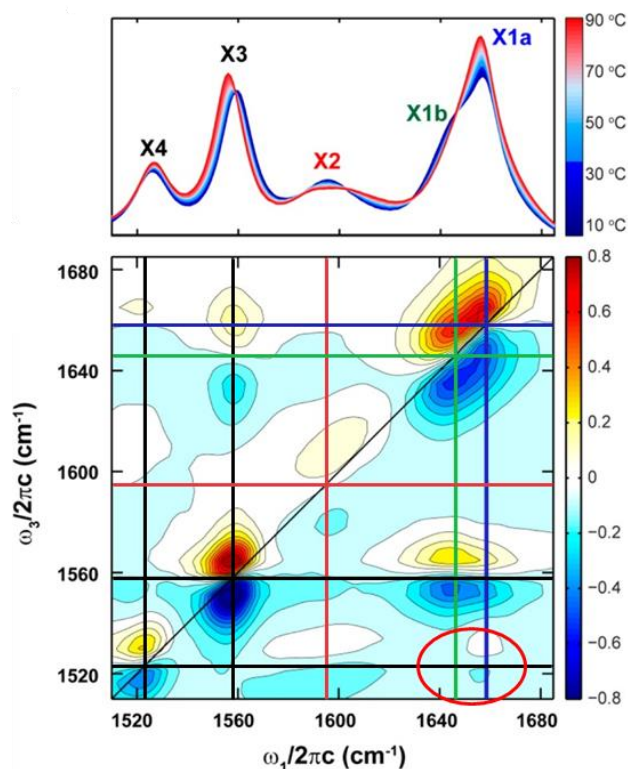


Figure 7. Structural model of  $\gamma$ D-crystallin illustrating <sup>13</sup>C-labeled N-terminal (yellow) and unlabeled C-terminal (blue) domains. 2D IR spectra of  $\gamma$ D-crystallin labeled with <sup>13</sup>C at the N-terminus are shown for (A) thermally-induced aggregates, (B) native, and (C) acid-induced aggregates. Reprinted with permission from Moran *et al.* *Protein Science*, 2014, **23**, 321 -331. Copyright © 2014 John Wiley and Sons.

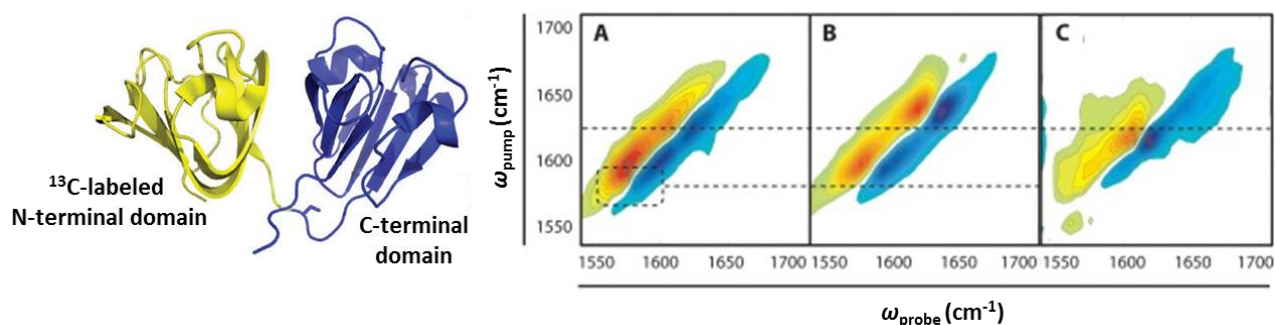


Figure 8. Structural model of HP35 showing residues labeled with CNPhe and 2D IR spectra of CNPhe in folded (upper panels) and guanidium-denatured (lower panels) HP35 at different waiting times.

Structural model: Reprinted with permission from Chung *et al.* *The Journal of Physical Chemistry B*, 2012, **116**, 11024 - 11031. Copyright © 2012 American Chemical Society. 2D IR spectra: Reprinted with permission from Chung *et al.* *Proceedings of the National Academy of Sciences of the United States of America*, 2011, **108**, 3578 – 3583.

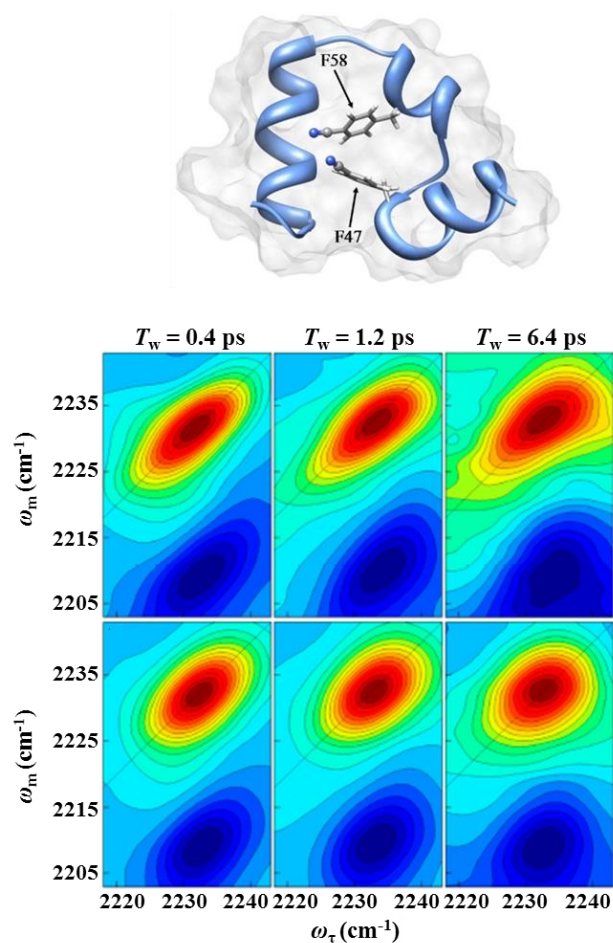


Figure 9. Structural model of a metal-carbonyl vibrational probe attached to hen egg white lysozyme and 2D IR spectrum of the metal-carbonyl frequency region. Reprinted with permission from King *et al.* *Journal of the American Chemical Society*, 2014, **136**, 188 - 194. Copyright © 2014 American Chemical Society.

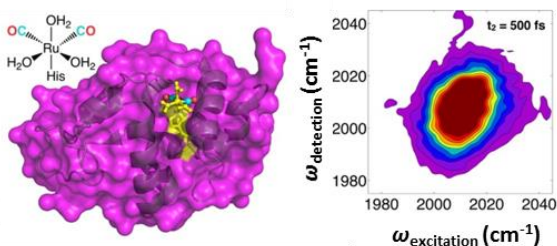


Figure 10. The structure of Re-carbonyl catalyst attached to a monolayer and example 2D IR spectrum. Rosenfeld *et al.* *Science*, 2011, **334**, 634 - 639. Copyright © 2011 American Association for the Advancement of Science.

